Nonstationary Analysis of the Directional Properties of Propagating Waves

M. A. DONELAN AND W. M. DRENNAN

National Water Research Institute, Burlington, Ontario, Canada

A. K. MAGNUSSON

Norwegian Meteorological Institute, Bergen, Norway

(Manuscript received 19 October 1995, in final form 13 March 1996)

ABSTRACT

It is proposed that the sea surface be studied in a way that takes into account the observed groupiness of wind-generated waves. A new method of analysis to study the directional properties of the surface is developed. It is demonstrated that this method, based on wavelet transforms, allows the instantaneous wave propagation directions at various frequencies to be estimated. Furthermore, the approach is shown to yield wavenumber spectra directly—a result of particular importance to such pursuits as remote sensing, gas transfer, and air–sea coupling.

1. Introduction

A record of the surface elevation at a point or a snapshot of the ocean surface reveals two important characteristics:

1) There is a definite underlying wavy structure, albeit strongly modulated and with superposed fine structure.
2) No section of the record of length greater than, say, three basic periods is duplicated elsewhere in the record.

These characteristics together suggest a random process in which elevation variance is distributed unevenly among frequency and wavenumber with a strong peak at some frequency/wavenumber and rapidly decreasing contributions away from the peak. The idea of a spectral representation of the statistical variability of the ocean surface was given formal expression by Pierson and Marks (1952), and is the basis for virtually all research and engineering studies of wind-generated sea waves. The idea is extremely appealing because, while it yields no prescription for predicting the occurrence of a particular sequence of events, it allows one to measure the average statistics of the process and to assign probabilities to the occurrence of wave heights and periods in a certain range (e.g., Longuet-Higgins 1952, 1983). Furthermore, since surface water waves are inherently dispersive, a spectral decomposition provides a convenient basis for calculation of, for example, wind forcing (Miles 1957 and ff; Phillips 1957; Makin 1979), wave–wave interaction (Phillips 1960; Hasselmann 1962 and ff), wave–bottom and wave–current interaction (Longuet-Higgins and Stewart 1964; Hasselmann and Collins 1968; Tolman 1991; Magnusson 1993), and wave dissipation (Hasselmann 1974; Phillips 1985; Donelan and Pierson 1987). Calculations of the directional properties of wind-generated waves (e.g., Donelan et al. 1985; Lygre and Krogstad 1986) are also predicated on the assumption that the wave field may be represented statistically by an average spectrum.

This surface wave model considers any realization of the sea surface to be composed of the sum of an infinite set of infinitesimal waves propagating with random phases and directions allocated such that the distribution of energy in frequency and direction agrees with the observed directional spectrum. The impressive success of this model of the ocean surface has tended to obscure its shortcomings. Key to this spectral representation model is the assumption of stationarity and ergodicity of the wave field (treated as a random process). These assumptions essentially preclude the use of standard spectral analysis techniques in unsteady conditions (i.e., during the growth of a wind sea) or during isolated events, such as a freak wave, *inter alia.* The common analytical approach is to omit these events, yet these very conditions are often the ones that are least understood and of the greatest practical concern.

In the following, an alternative model of the sea surface is presented. Based on this model, a new method

Corresponding author address: Dr. M. A. Donelan, National Water Research Institute, Canada Centre for Inland Waters, P.O. Box 5050, Burlington, Ontario L7R 4A6, Canada.
E-mail: mark.donelan@cciw.ca

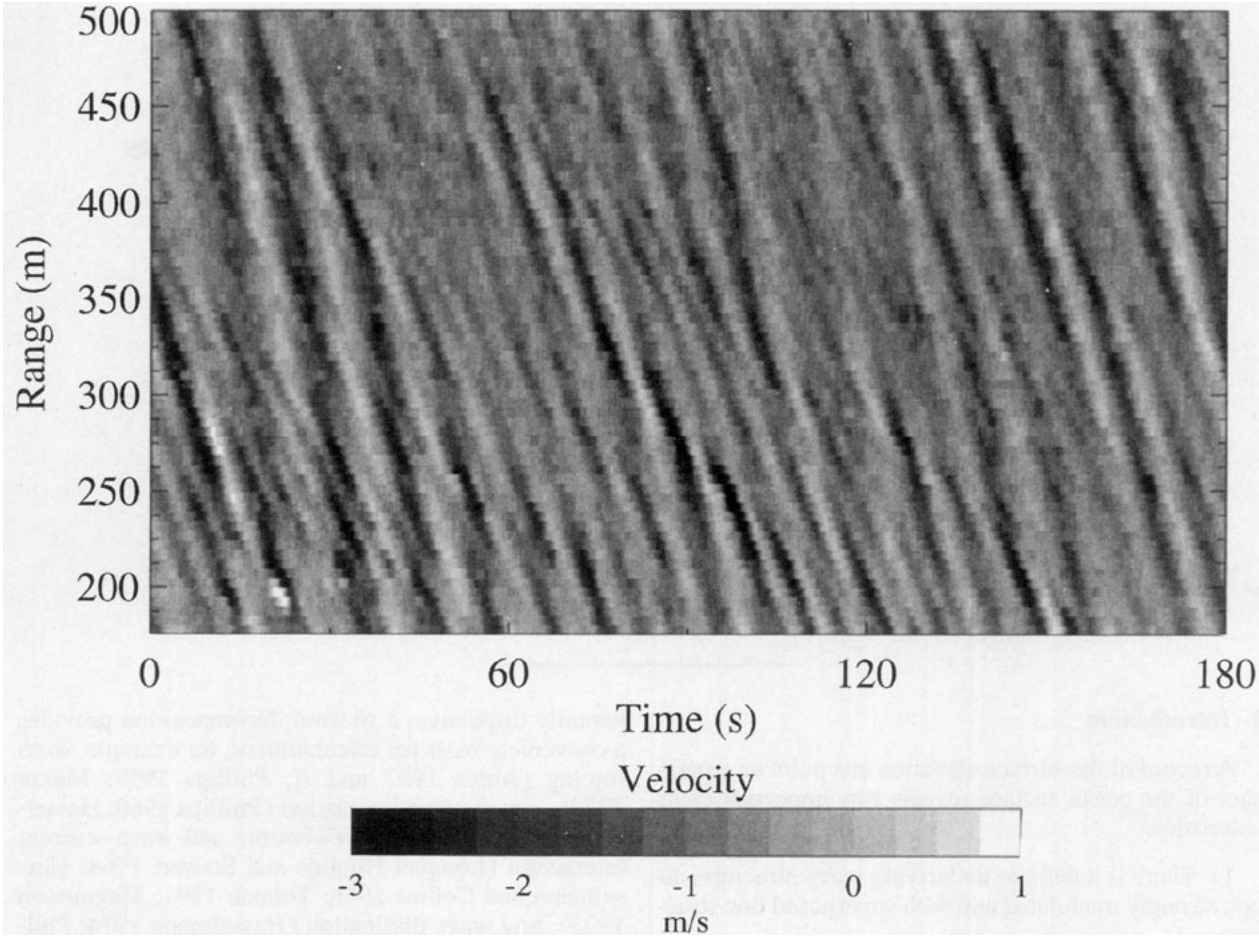

FIG. 1. Surface velocity variations during a 3-min interval from an S-band frequency-modulated continuous wave radar directed into the wind. The dark stripes correspond to wave crests propagating toward the radar. From Poulter et al. (1995).

of analyzing the sea surface is developed. Results from this new method, the wavelet directional method (WDM), are compared to those of the more traditional maximum likelihood method. Field data are analyzed and the directional properties of wave groups within the record are studied. It is also shown that the new method yields wavenumber spectra.

2. A group model

The idea that the sea surface may be represented by the superposition of wave groups of varying amplitude, group shape, and group velocity was first advanced by Mollo-Christensen and Ramamonjiarisoa (1978). Inspired by the envelope solitons of Yuen and Lake (1975), they proposed a model in which groups of Stokes-like waves propagate without change of form. Interactions between groups were assumed to be negligible. The observed spectrum arises through a random distribution of the amplitudes, propagation directions and phases of these groups. Although the solution of the nonlinear Schrödinger equation gives rise to an envelope of sech^2 shape (Hui and Hamilton 1979), for simplicity the groups were given Gaussian envelopes and were described by

$$w_p(x, y, t; \phi) = \exp\left(-\frac{(x - Vt)^2}{2l^2} - \frac{y^2}{2h^2}\right) \times \sum_{n=1}^{\infty} a_n \cos n(k_1 x - \omega_1 t - \phi), \quad (1)$$

where x is the propagation direction, V the (nonlinear) group velocity, and l and h are horizontal scale parameters for the group shape. The Fourier series describes the Stokes-like frequency distribution with all the components having the phase speed of the fundamental: $c(k) = c(k_1) = \omega_1/k_1$. The group velocity and wavenumber may differ from the linear theory values. The subscript p denotes permanency of group shape.

The permanency of the above groups depends on a subtle balance among amplitudes of the spectrum. If

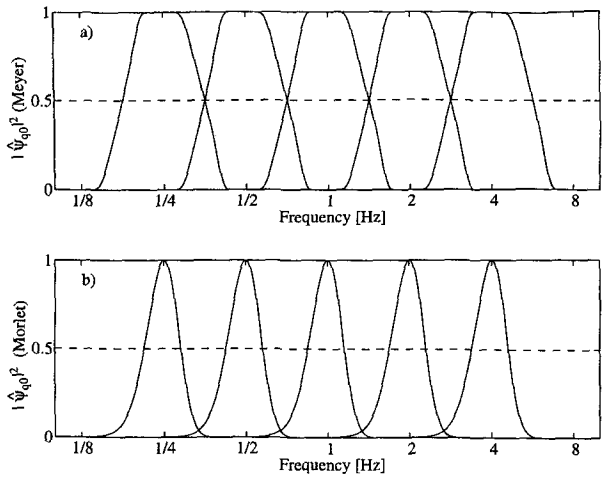

FIG. 2. Fourier space plots of $|\hat{\psi}_{q0}|^2$ for $q = -2, -1, 0, 1, 2$. Meyer and Morlet wavelets in panels (a) and (b) respectively.

the amplitude of the envelope of these groups is too small or too large compared to the wavelength of the fundamental component, the groups will not be of permanent form. However, through coalescence and dispersion of the various components, groups may exist over a finite interval in space and time. Pierson et al. (1992) have demonstrated that a sufficiently steep group will propagate for a short time without a perceptible change of form.

One can think of the sea surface as a collection of such groups randomly distributed with a probability such that the average spectrum has the observed characteristics of a sharp forward face, an equilibrium range and suitable spreading about the wind direction. A formal statement of the treatment of a sea consisting of wave groups, rather than infinitesimal wave trains, has been given by Komen et al. (1994, section I.2.6).

We envisage the sea surface consisting of a random collection of groups propagating in various directions and having different levels of energy or envelope steepness. Groups of low steepness are approximately linear and evolve over time and space: groups may steepen (coalesce) or flatten (disperse) depending on phasing of component waves in any time/space interval. The steepest groups exhibit Stokes-like harmonics, such as that modeled by (1). Ramamonjiarisoa (1974) and Mollo-Christensen and Ramamonjiarisoa (1978) give evidence for the existence of groups of type (1), and Donelan et al. (1985) have shown that the balance of "bound" (Stokes like) harmonics and free waves depends on the intensity of wind forcing, U/c_p.

Radar observations (e.g., Poulter et al. 1995) and acoustic mapping of the surface from beneath (Farmer and Vagle 1988) have indicated the presence of directed groups propagating for several periods in a given direction. These observations have also confirmed the modulated group breaking structures first noticed by Donelan et al. (1972). Figure 1 (reprinted from Poulter et al. 1995) illustrates the group structures in a wind-driven wave field. Such time-range data displays yield information that is not available from point measurements. Horizontal slices correspond to the usual time histories at a point that could be obtained by, for example, a moored accelerometer. Vertical slices are the instantaneous "topography" of surface velocities along the radar look direction, which in this case is into the wind. The slope of dark (or light) lines corresponds to the component of phase velocity toward the radar, while the group velocity component may be estimated from the slope of lines joining the centers of successive crest/trough (dark/light) traces. The most pronounced features show the characteristic deep water (here, depth > 100 m) relation between phase and group velocity. The offwind propagation angle may, in principle, be estimated from the apparent wavelength (vertical separation between parallel crest lines) and the theoretical wavelength deduced from the period (horizontal separation between parallel crests). Coherent group patterns over many periods and the observed range of 325 m correspond to wave groups propagating toward the radar or at a small angle to the radar look direction. Groups propagating at large off-range angles appear for relatively short space-time intervals—depending on degree of long-crestedness—and several of these may be discerned on the figure. Of course, this presentation emphasizes the largest waves, which have the largest orbital velocities, and these are generally narrowly focused in the wind direction under these steady wind, long fetch, deep water conditions.

The common method of wave observation—time histories at a point, corresponding to horizontal slices in Fig. 1—does not yield any information about the coherence of groups. A run of high waves may occur through random superposition of time independent components—the assumption inherent in Fourier analysis of time series—or may be caused by the passage of groups of waves in which the energy is concentrated in a small range of wavenumbers along particular space–time trajectories. Radar derived displays, such as Fig. 1, provide powerful evidence for the latter.

These observations of strongly modulated coherent groups lead us to suggest a new model for the propagation characteristics and energy distributions of waves in a wind-generated sea. We postulate the propagation of waves in groups having a narrow range of variation of wavenumber magnitude and direction within a group. Groups of various wavenumber ranges and directions may coexist. The statistical average of the propagation characteristics of a sea is called a directional spectrum. Energy may be concentrated near particular vector wavenumbers at any instant (or position). Over time (or space) the variability of the spectrum arises from the passage of groups with various amplitudes and vector wavenumbers.

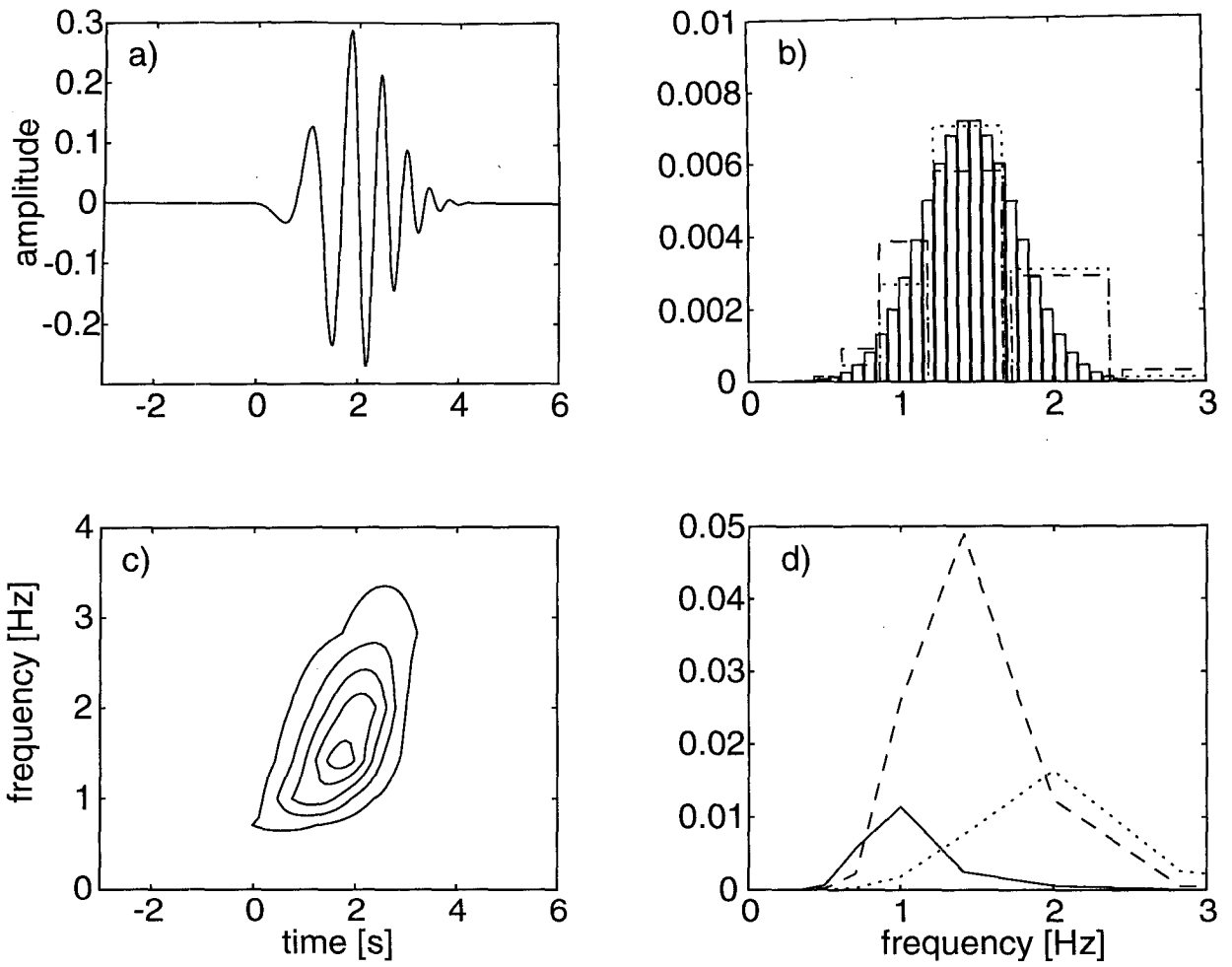

FIG. 3. A comparison of Fourier and wavelet analyses of an isolated dispersing Gaussian wave group. The time series of the group is illustrated in panel (a). In (b), the solid line bars show the Fourier spectrum, while the dashed and dotted bars show the Meyer and Morlet wavelet spectra of the full time series. In (c), a contour plot of $|W_{qp}|^2$ is shown on the same timescale as (a), while in (d) wavelet energy spectra $|W_{qp}|^2$ versus f_q for p corresponding to times of 0.5 s (solid line), 1.5 s (dashed), and 2.5 s (dotted) are shown.

3. The wavelet directional method

In order to test our hypothesis we need a nonstationary method of analysis of wave records that will be capable of decomposing the space/time ($\mathbf{x}$, t) observations into a frequency (or wavenumber)/time frame. Fourier analysis is clearly inadequate in that it sacrifices all temporal resolution within a given block for excellent frequency resolution. Recently developed wavelet analysis techniques (e.g., see Farge 1992 or Kaiser 1994), on the other hand, are ideally suited to this purpose. Wavelet analysis allows for good temporal and frequency resolution, although there is considerable loss of frequency resolution compared to Fourier analysis. Recall that the radar principle (or Shannon's uncertainty principle) limits the product of time resolution and frequency resolution, so that an increase in one must be at the expense of the other.

In wavelet analysis, one defines a mother wavelet $\psi(t)$ (meeting certain integrability requirements in the Hilbert space $L^2(R)$—see Kaiser 1994), and then considers the set of translations and dilations of this mother wavelet, $\psi_{qp}(t) = 2^{q/2}\psi(2^q t - p)$, where q, p are integers. Note that p serves as a surrogate for time. The convolution of this family of wavelets with time series $G(t)$ yields the coefficients W_{qp}, each with information about $G(t)$ at scale 2^q and time p. This is analogous to Fourier analysis where by convolving $G(t)$ with the family of functions $e^{-i\omega_q t}$, one determines the frequency spectrum $\hat{G}(\omega_q)$. Since the family of functions $e^{-i\omega_q t}$ also form a basis for functions in L^2, one can, of course, write $G(t)$ as a combination of these functions in the standard way. In a similar fashion, one can choose certain mother wavelets such that the ψ_{qp}s form a basis in L^2. In this case, $G(t) = \Sigma_q \Sigma_p W_{qp}\psi_{qp}$. We distinguish here be-

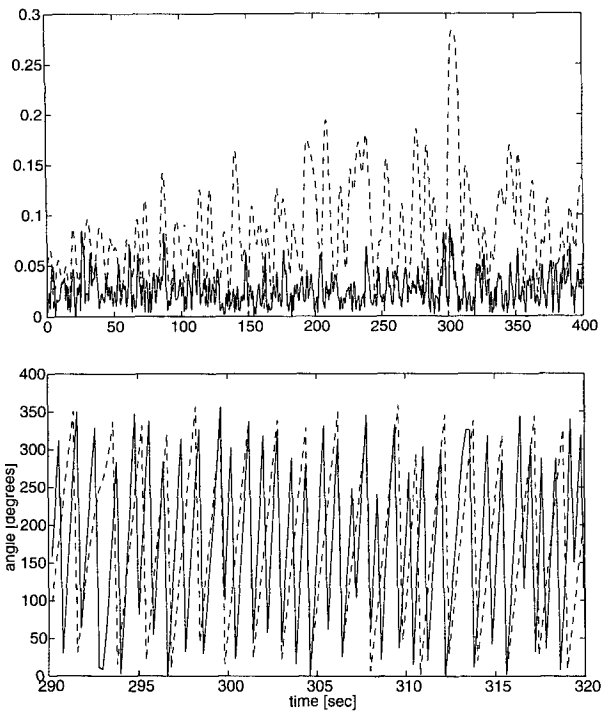

FIG. 4. An example of a wavelet transform of surface elevation at a point. The upper and lower panels show respectively the amplitude and phase of a frequency component at the peak frequency (- - -) and twice the peak frequency (——).

tween the *frequency* information resulting from Fourier analysis and *scale* information resulting from wavelet analysis. As we will see below, how closely the two are related depends on the properties of ψ. It is more convenient to calculate the W coefficients in frequency space, using $W_{qp} = \text{ifft}(\hat{G}\hat{\psi}_{qp})$, where $\hat{\psi}$ is the fft of ψ and [i]fft means [inverse] fast Fourier transform.

It is clear that there are many possible choices for the mother wavelet ψ, and indeed, a variety have been introduced into the literature (see Kaiser 1994). Farge (1992) in her review of wavelets in turbulence research makes the important point that the W_{qp}s contain information not only on G, but also on ψ, hence it is important to choose a wavelet that is in some sense suited to the physical quantities to be studied.

We investigate here two mother wavelets, the Meyer and Morlet wavelets, recently introduced into air–sea related fields. Meyer (1989) proposed an algorithm by which a family of orthogonal wavelets, spanning (and thereby forming a basis for) L^2, could be generated. Hayashi (1994), studying atmospheric turbulence, implemented the algorithm, defining the mother wavelet in Fourier space $\hat{\psi}$, as

$$\hat{\psi}(\omega) = \exp(-i\omega/2)[\hat{\phi}(\omega/2)^2 - \hat{\phi}(\omega)^2]^{-1/2} \quad (2)$$

$$\hat{\phi}(\omega) = [g(\omega)g(-\omega)]^{-1/2} \quad (3)$$

$$g(\omega) = h(4\pi/3 - \omega)/[h(\omega - 2\pi/3) + h(4\pi/3 - \omega)] \quad (4)$$

$$h(\omega) = \exp(-2/\omega^2) \times (\omega > 0), \quad (5)$$

where $(\omega > 0)$ is 1 if true and 0 if false. We note that our expression for h is different from that of Hayashi (1994) by the addition of a normalization factor of one-half in the denominator. This scales $|W_{qp}|^2$ to represent spectral power, analogous to that derived from the Fourier coefficients. In Fig. 2a, we plot $|\hat{\psi}_{q0}|^2$, for $q = -2$, -1, 0, 1, 2, corresponding to the scales of 1/4, 1/2, 1, 2, and 4 Hz. The following points should be noted from the figure: First, although at a given scale, for instance 1 Hz ($q = 0$), the wavelet is clearly centered at that frequency, it contains information at neighboring frequencies as well. This is, in essence, the distinction between frequency and scale made above: a scale is an average weighted over neighboring frequencies. Second, $\Sigma_q |\hat{\psi}_{q0}|^2 = 1$, as must be the case for orthogonal wavelets. Although the Meyer wavelets have found application in the analysis of atmospheric turbulence (Hayashi 1994), they are not particularly well suited to our present work due to their relatively poor frequency resolution for a given scale.

Although nonorthogonal, Morlet wavelets (see Grossman and Morlet 1984) with the mother wavelet defined by $\psi(t) = \exp(ict)\exp(-|t|^2/2)$, c a constant, are well localized in both time and frequency. Furthermore, their Gaussian envelope shape makes the Morlet wavelet a natural choice for ocean wave analysis (see, e.g., Chapron et al. 1996). In Fig. 2b, we plot $|\hat{\psi}_{q0}|^2$, for $q = -2, \cdots, 2$, calculated using the Morlet wavelets. The improvement in frequency resolution compared with the Meyer results of Fig. 2a is evident. It is also evident that $\Sigma_q |\hat{\psi}_{q0}|^2 \leq 1$. In particular, midway between wavelet scales, Morlet wavelets tend to lose most of the energy in the signal. It is therefore common to carry out Morlet wavelet analysis with additional intermediary scales or "voices," so that, for example, $q = \cdots, -1, -1/2, 0, 1/2, 1, \cdots$. These additional voices are largely, but not fully, independent of the integer scales. As the number of voices is further increased, the independence of neighboring voices is clearly reduced. In what follows below, the Morlet wavelet is used for the bulk of the analysis, although the Meyer wavelets are also applied to provide an indication of the effects of the choice of wavelet on the results.

Prior to proceeding with the main results, we provide a brief example of the different results gained from Fourier and wavelet analysis. Consider the time series $G(t)$ consisting of the isolated dispersing wave group given by

$$G(x,t) = -\frac{A}{D^{1/4}}\exp\left[-\frac{4\omega_0^2 B^2}{g^2 D}\left(x - \frac{gt}{2\omega_0}\right)^2\right] \times \sin\left(\frac{\omega_0^2 x}{Dg} - \frac{\omega_0 t}{D} - \frac{4B^4 t^2 x}{Dg} + \frac{1}{2}\tan^{-1}\frac{4B^2 x}{g}\right), \quad (6)$$

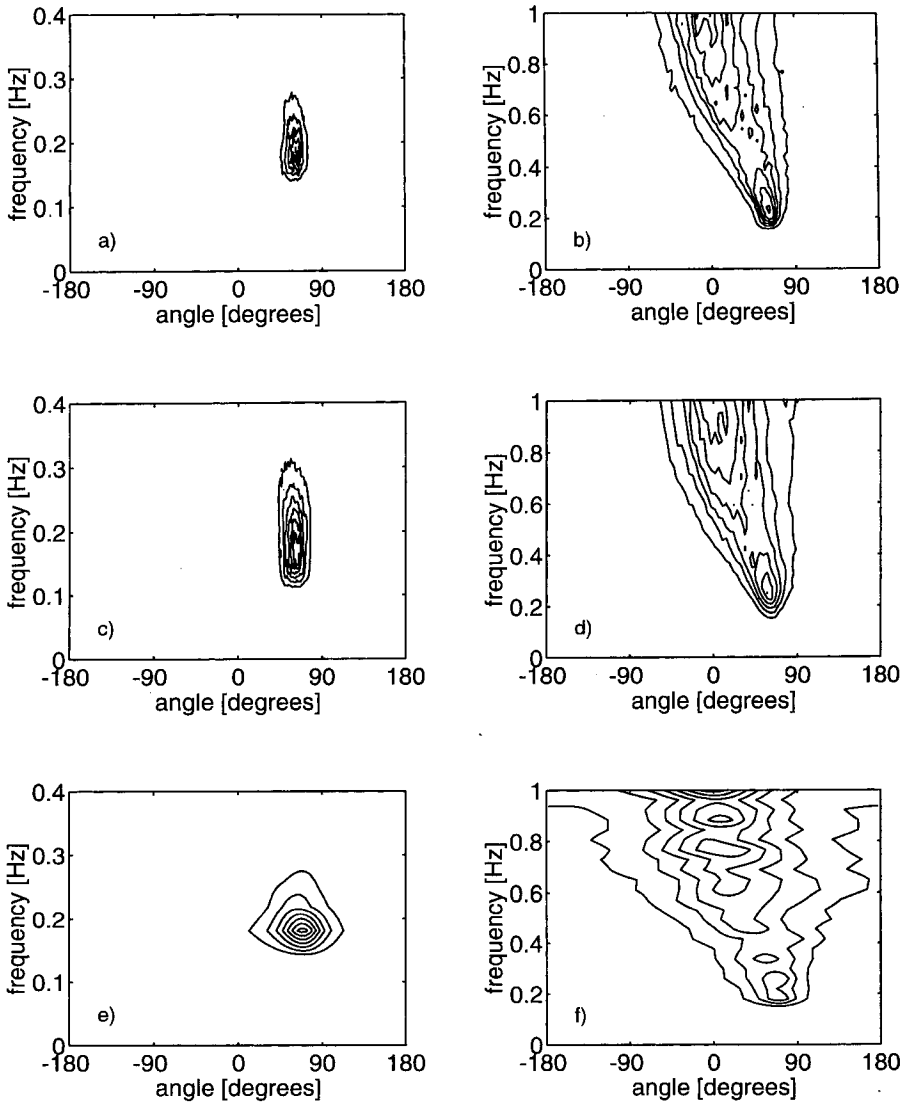

FIG. 5. Frequency–direction spectra for a well-developed wave field (run 87062). Panels (a), (c), and (e) are the contour plots of the spectrum via the WDM using Morlet wavelets, WDM using Meyer wavelets and MLM respectively; panels (b), (d), and (f) are the corresponding spectra multiplied by f^5.

where $B = 2$ is the envelope decay constant, $x = 1$ the fetch, $A = 0.4$ the amplitude, $D = 1 + (16B^4x^2/g^2)$, and $\omega_0 = 3\pi$. This is the classic dispersing two-dimensional Gaussian group of Neumann and Pierson (1966). The time series of G is shown in Fig. 3a, along with its Fourier frequency spectrum in Fig. 3b, with each solid (line) bar representing the energy in a discrete frequency bin. In Fig. 3c, a contour plot of the magnitude squared of the (Meyer) wavelet transform coefficients, $|W_{qp}|^2$, ($q = -2, -3/2, -1, \cdots, 3$) on frequency/time axes is shown. The passage of the wave group is readily identified, as is the frequency upshifting which occurs as the faster long waves lead the slower short ones. This time localization is the advantage of wavelet analysis over Fourier analysis. The compromise comes in a loss of frequency resolution. In Fig. 3d, we plot wavelet spectra at times 0.5, 1.5, and 2.5 s. The increase in frequency and change in local energy as the group passes are clearly seen, although there are only six fully independent (logarithmically spaced) frequency bands. The spectrum derived by averaging the wavelet energy over the full time record is shown using dashed bars in Fig. 3b. Note that the wavelet points identify scales, that is, averages of frequencies around some center frequency. The dotted bars show the spectrum derived from the Morlet wavelet: the Morlet scales are seen to be closer to the true frequency (i.e., the energy follows more closely the Fourier spectral energy) than the Meyer scales.

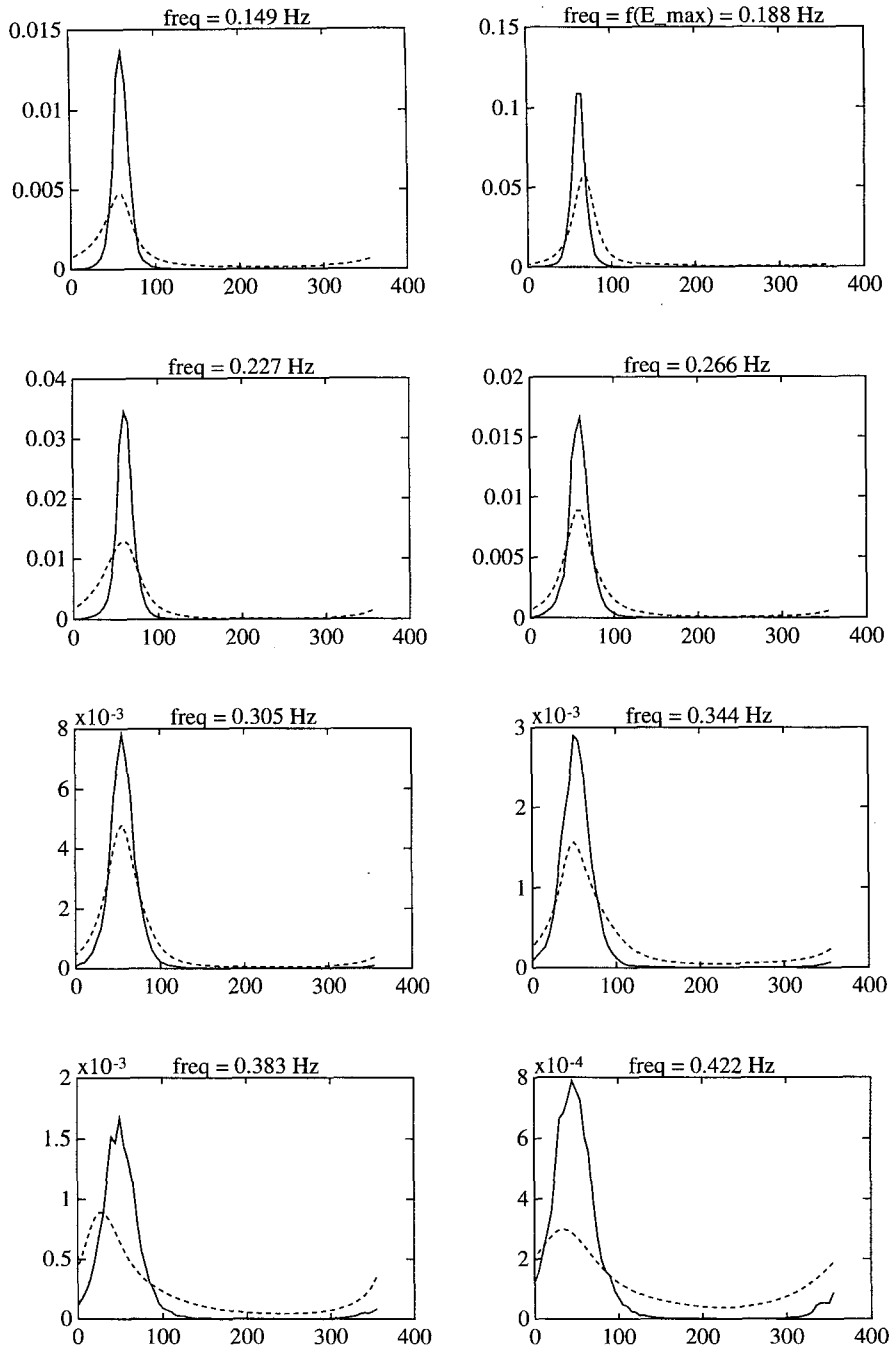

FIG. 6. Directional distributions at various frequencies for run 87062.
WDM (——); MLM (- - -).

The most reliable data for analyzing the directional properties of waves is that obtained from arrays of wave staffs. The method we will describe here is written with these data in mind. Consider a set of time series obtained from an array of n wave staffs: $\eta_i(t)$, $i = 1, \cdots, n$. The first step is to obtain the (complex) wavelet transform of these n datasets at m discrete frequencies f_q, $q = 1, \cdots, m$: W^i_{qp}, $i = 1, \cdots, n$. Thus, for each chosen frequency f_q, we now have a time series of the amplitude and phase of that component (Fig. 4). Pairs of wave staffs (i and j) yield measured phase differences ϕ_{ij}:

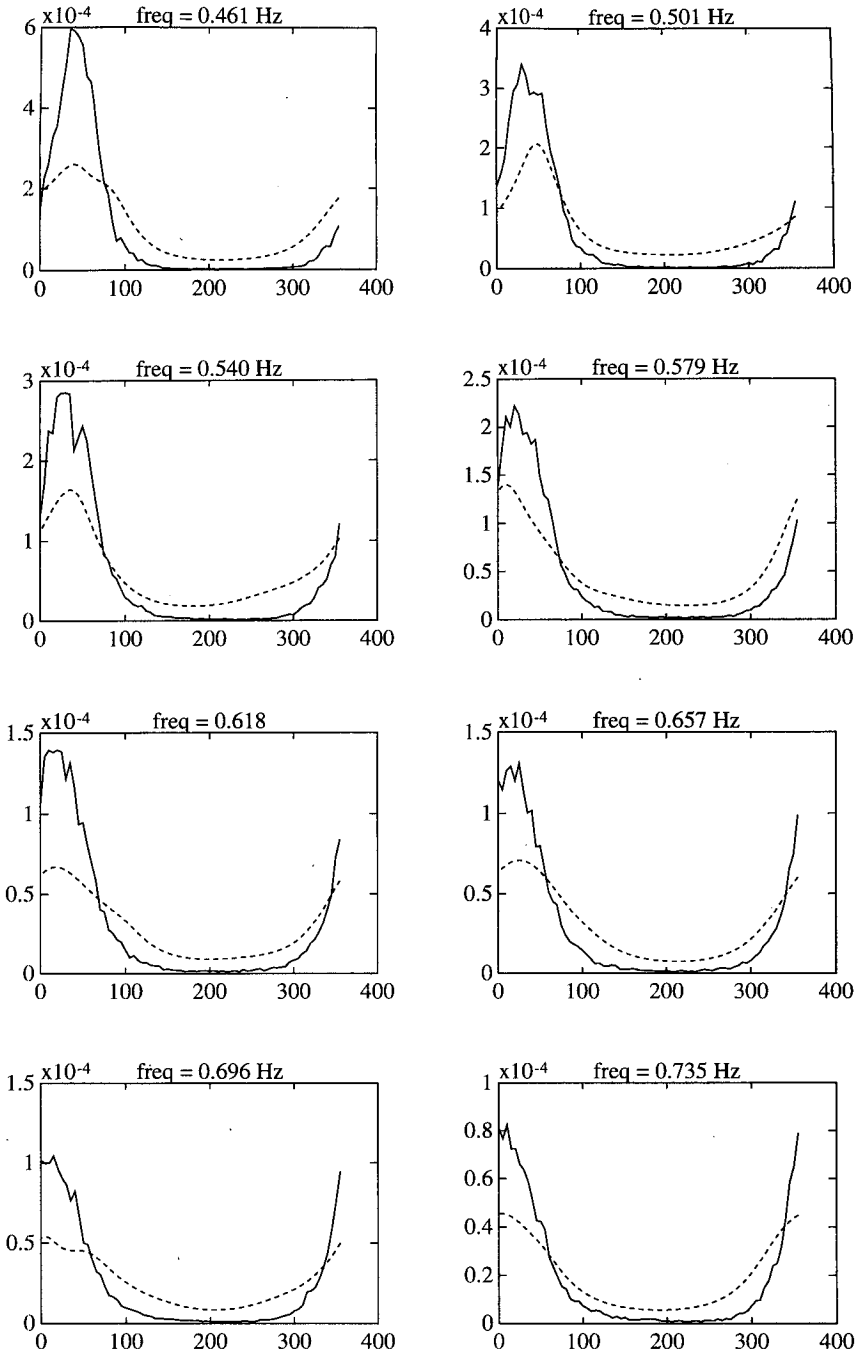

FIG. 6. (*Continued*)

$$\phi_{ij} = kr_{ij}\cos(\theta - \alpha_{ij}), \tag{7}$$

where $\mathbf{r} = (r, \alpha)$ are the separation vectors of pairs of staffs, and $\mathbf{k} = (k, \theta)$ is the wavenumber vector at the chosen frequency and time.

It is easily shown that the wavenumber vector may be determined from two pairs of staffs by

$$k = \left[\frac{\phi_{ab}}{r_{ab}}\sin\alpha_{cd} - \frac{\phi_{cd}}{r_{cd}}\sin\alpha_{ab}\right] \Big/ [\sin(\alpha_{cd} - \alpha_{ab})\cos\theta] \tag{8}$$

$$\theta = \arctan[(\Gamma\cos\alpha_{cd} - \cos\alpha_{ab}) / (\sin\alpha_{ab} - \Gamma\sin\alpha_{cd})], \tag{9}$$

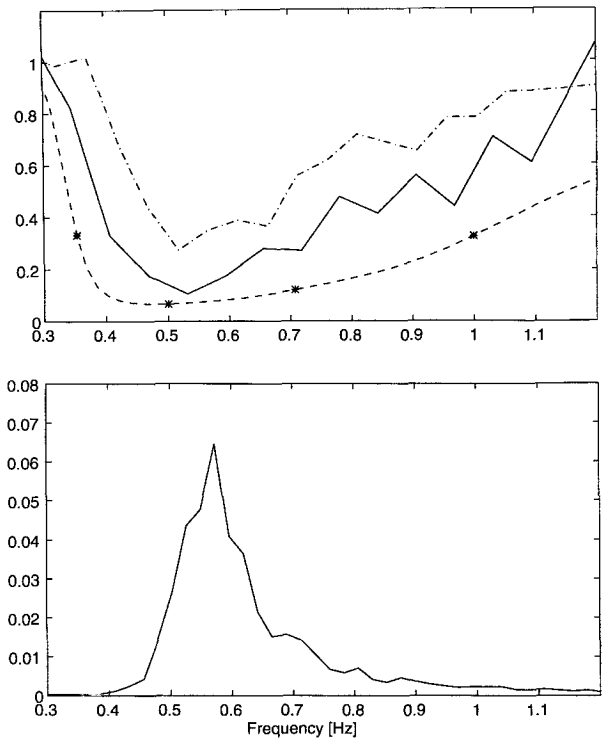

FIG. 7. The ratio of cross-wave slope spectra to alongwave slope spectra for run 87082 from the data (——), via WDM (— — —), and via MLM (— · —), upper panel. The stars on the WDM curve show the (mostly) independent scales. In the lower panel, the 1D wave spectrum shows where the spectral energy is concentrated.

where $\Gamma = (\phi_{ab}/\phi_{cd})(r_{cd}/r_{ab})$ and the pairs *ab* and *cd* are chosen so that the angular difference between their separation vectors $(\alpha_{ab} - \alpha_{cd})$ is close to 90° or 270°. If there are more than two pairs (i.e., more than three wave staffs) multiple estimates of $\mathbf{k}$ are obtained and the means and standard deviations of the estimates of $\mathbf{k}$ may be calculated. Finally, the directional spectrum is calculated by binning the energy (amplitude squared of W^i_{qp}) at each time into the calculated wavenumber bin.

4. Results

Perhaps the most widely accepted means of computing directional spectra from arrays of wave staffs is the maximum likelihood method (MLM, e.g., Capon 1969). In the following we compare estimated directional spectra from the two methods. In order to compare the results of our new method with conventional approaches, we ignore the wavenumber magnitude and examine the distribution of energy in frequency and direction integrated over time. We examine data acquired from the research tower in Lake Ontario (Donelan et al. 1985) during the WAVES Experiment (Tsanis and Brissette 1992) in 1987. The research tower stands in 12 m of water at the western end of Lake Ontario. Strongly forced conditions occur in strong west winds over the minimum fetch of 1.1 km, whereas weaker east winds yield waves approaching full development over a fetch of some 300 km. Two cases are selected for illustration: (i) run 87062, which is near full development, and (ii) run 87082, which is strongly forced. The data are obtained from an array of 6 capacitance wave staffs arranged in a centered pentagon of radius 25 cm and sampled at 20 Hz. There were 105 pairs of which 35 had included angles within 20° of either 90° or 270°. These 35 pairs form the basic dataset.

a. Frequency-direction spectra

Contour plots of the frequency–direction spectra are illustrated in Fig. 5 for the well-developed case, run 87062. In panels (a) and (c), we compare spectra derived via the WDM using Morlet and Meyer wavelets respectively in order to test how sensitive the results are to the particular wavelet used. The right-hand panels, (b) and (d), show the same two spectra multiplied by f^5 to enhance the high frequency contributions. Comparing (a) and (c), we see a very similar directional distribution, but with the Meyer wavelet producing spectra somewhat wider in frequency. This is expected, as seen in Fig. 2 and the discussion above. In the remainder of the paper, we confine our attention to the use of the Morlet wavelet in the WDM. The MLM spectrum appears in panels (e) and (f), the latter multiplied by f^5. Comparing the WDM and MLM spectra, good agreement in the mean propagation directions is seen, but the wavelet directional method shows appreciably less spreading than the MLM at all frequencies. This is emphasized by comparing panels (b) and (f). Both methods show the turning of the waves toward the wind direction at high frequencies, while the low frequencies tend to come from the long fetch direction (70°). This phenomenon was first described by Donelan et al. (1985). It is also apparent that the WDM is far smoother than the MLM although both have been treated in the same way in the contouring process.

A clearer view of these aspects of the WDM and MLM spectra can be seen by examining the set of slices across direction at particular frequencies shown in Fig. 6. The MLM (dashed) is consistently broader than the WDM, and, at frequencies of twice the peak and above, indicates significant energy in waves propagating against the wind. Whereas the WDM shows a consistent increasing trend in the spreading and a slow transition of the energy toward the wind direction (0°) with increasing frequency, the MLM shows significant random fluctuations in both of these aspects.

The question arises as to which of the two methods best represents the actual spreading in the data. In Fig. 7 we plot the ratios of cross-wave and alongwave slope spectra at each frequency for the MLM and WDM spectra. At a given frequency, the wavenumbers cancel, and the ratio is given by

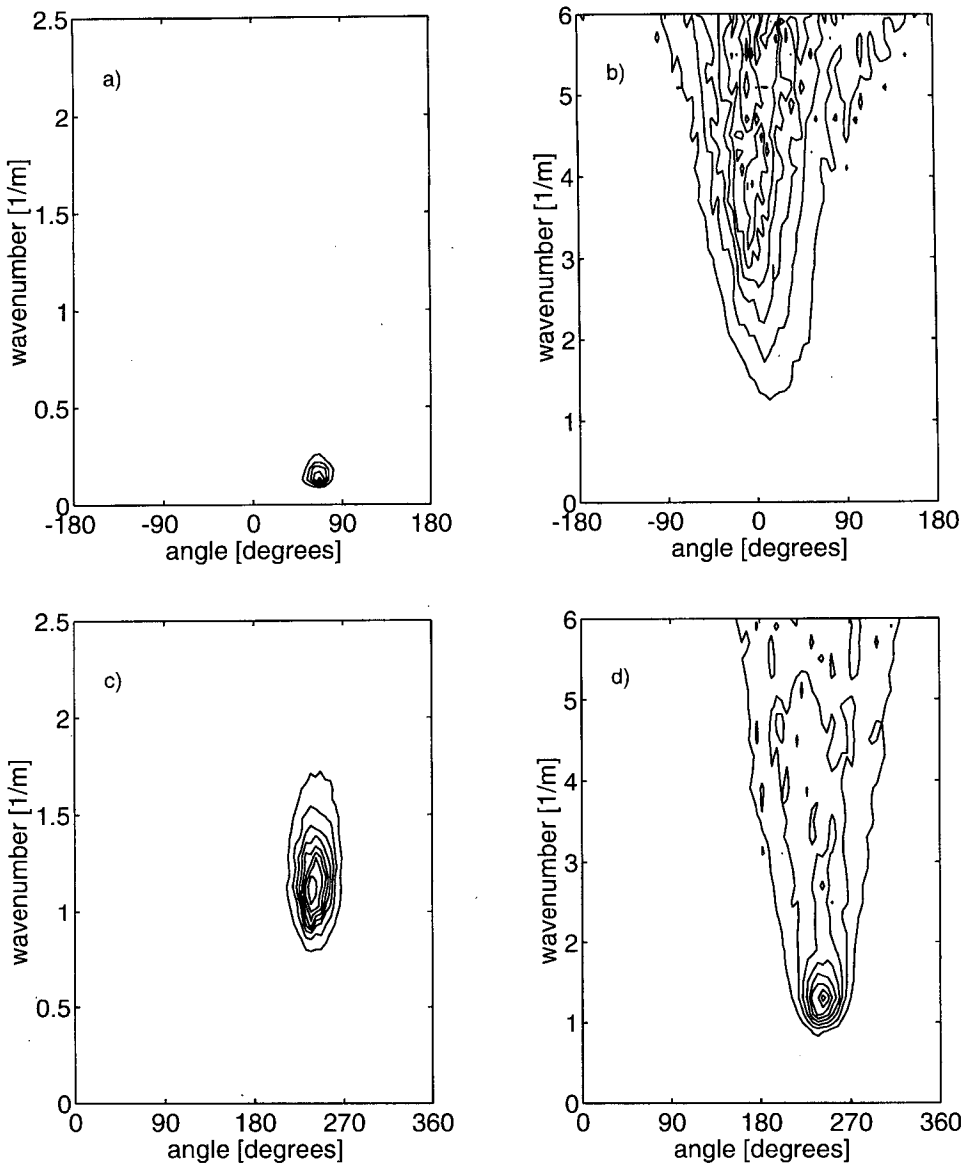

FIG. 8. Wavenumber spectra. Panels (a) and (c) are contour plots of the spectrum for runs 87062 and 87082 respectively; panels (b) and (d) are the corresponding curvature spectra.

$$\int_0^{2\pi} \sin^2(\theta - \theta_0) D(\theta) d\theta \Big/ \int_0^{2\pi} \cos^2(\theta - \theta_0) D(\theta) d\theta, \quad (10)$$

where $D(\theta)$ represents the normalized directional energy distribution and θ_0 the mean wave direction at the frequency. We can make a similar calculation from the data, calculating the alongwave and cross-wave slopes spectra from the wave staff time series by fitting a second-order surface to the six elevation estimates at each time step. The instantaneous two orthogonal directions are then readily computed and may be rotated into and normal to the wave direction (see Tsanis and Brissette 1992). This slope ratio is also plotted in Fig. 7. The WDM spreading closely approximates the actual spreading near the spectral peak but is seen to underestimate the spreading at higher frequencies. There is insufficient energy at lower frequencies for a comparison to be made. The MLM spreading, on the other hand, is consistently too large, overestimating the crosswave/alongwave spectral ratio near the peak by a factor of over 2. The underestimate of the WDM at higher frequencies is not unexpected. It is a result of the inability of the WDM to resolve two or more waves

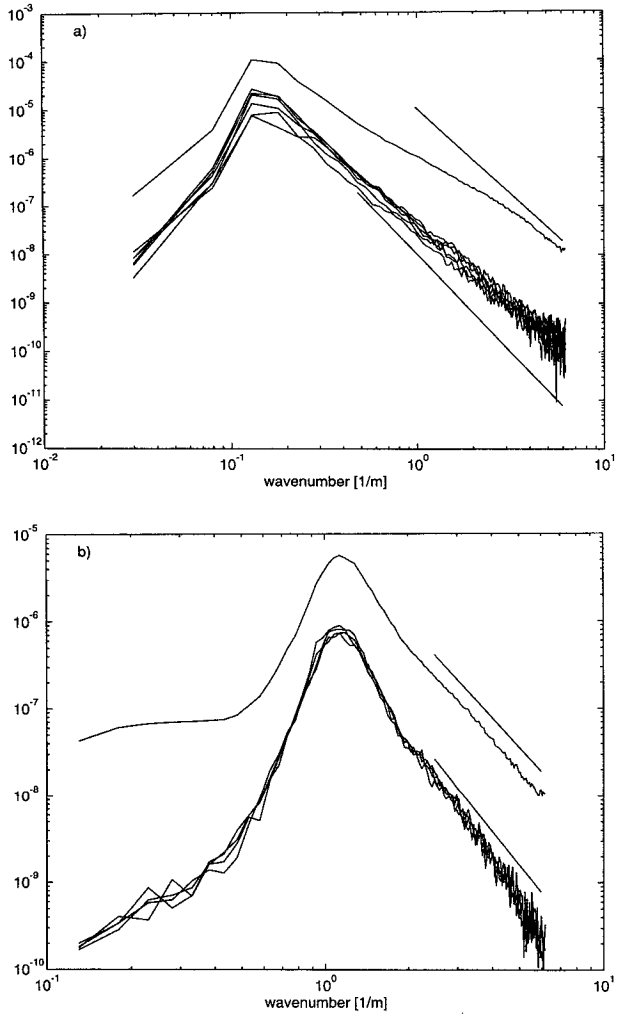

FIG. 9. One-dimensional spectra (upper curve) and several slices through the wavenumber-frequency spectrum in and near the wind direction. The straight lines show slopes of $k^{-3.5}$ (upper curve) and k^{-4} (lower curve). The upper and lower panels are from runs 87062 and 87082 respectively.

of the same wavenumber passing over the array at the same time.

b. *Wavenumber spectra*

The method proposed here yields wavenumber spectra directly and it is this form that is useful for most purposes. Since our data are obtained from observations at fixed points and are first decomposed by a wavelet time-frequency analysis, we are left with a distribution of energy in various wavenumbers at each chosen frequency-of-encounter band. Waves having different wavenumbers contribute to a particular frequency band depending on the local currents and orbital velocities; that is, they are Doppler shifted in and out of a given frequency band as the local currents change (Ataktürk and Katsaros 1987). However, we are able with this method to assign a wavenumber vector to the amplitude at each instant in a particular frequency band. The overall distribution of these wavenumber-tagged amplitudes (squared), integrated over time, is the wavenumber spectrum. This is shown for the two illustrative cases in Fig. 8. Panels (a) and (c) show the direct wavenumber spectra, and panels (b) and (d) the spectra $\times k^4$ or the "saturation" parameter (Phillips 1985). In Fig. 9 the one-dimensional wavenumber spectra are shown (integrated over direction) and also a series of slices of the wavenumber spectra in directions close to the wind direction. In the strongly forced case (Fig. 9b) the one-dimensional spectrum shows a distinct region above the peak having a slope of $k^{-3.5}$, in agreement with the generally accepted f^{-4} shape of the frequency spectrum (Toba 1973; Donelan et al. 1985). The corresponding slices through the spectrum in the wind direction have slopes close to k^{-4}, as originally conjectured by Phillips (1958). The difference in slope is explained by the increased spreading with wavenumber above the peak (Donelan et al. 1985). At higher wavenumbers the spectra fall off slightly. The data were gathered at 20 Hz and averaged to 2.5 Hz so that the analysis was carried out to a Nyquist frequency of 1.25 Hz, corresponding to a wavenumber of 6.29 m^{-1}. However, Doppler shifting spreads the energy at each wavenumber over various frequencies, so that some energy at wavenumbers just below the Nyquist wavenumber would be observed at frequencies above the Nyquist frequency and is therefore not captured here. The increased slope is probably due to this.

The well-developed case (Fig. 9a) shows much the same behavior, but the k^{-4} region is well above the

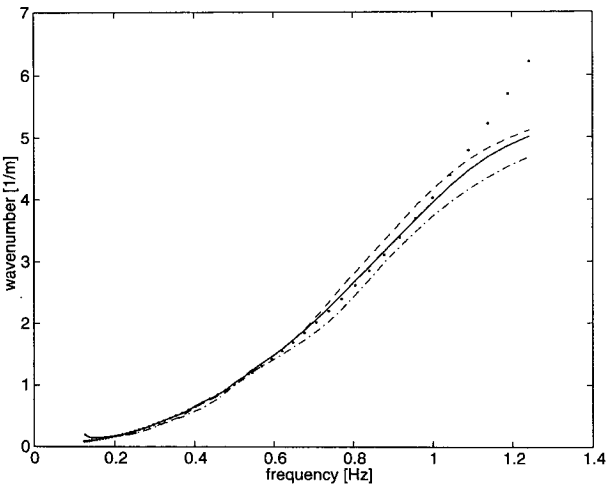

FIG. 10. Wavenumber–frequency diagram for run 87062: $\bar{k}$ versus frequency for the whole time series (solid line), in the wave crests [$\eta > (\overline{\eta^2})^{1/2}$; dot–dash] and in the wave troughs [$\eta < -(\overline{\eta^2})^{1/2}$; dashed]. Linear theory is shown by a series of dots.

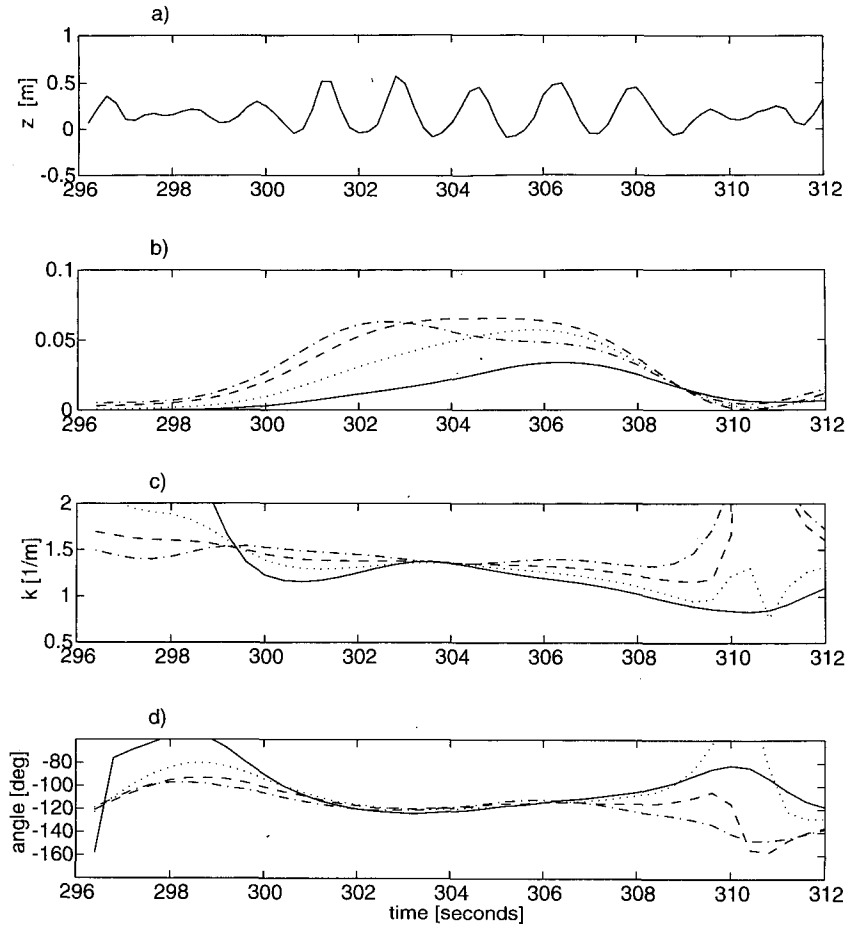

FIG. 11. Panel (a): the passage of a group in the time history of surface elevation. Panels (b), (c), and (d): the evolution of amplitude, wavenumber, and direction of the frequency bands that constitute the group. The frequencies 0.50, 0.55, 0.60, and 0.65 Hz are represented by solid, dotted, dashed, and dot–dashed lines respectively. Note that while adjacent frequencies are somewhat dependent, the first and last are virtually independent.

peak, reflecting the weak forcing near the peak and a "saturated" spectrum only in the high wavenumber slowly moving part of the spectrum.

c. *The dispersion relation*

The dispersive properties of the waves can be readily examined with this method. Figure 10 shows a plot of the average wavenumber in each frequency band versus frequency for the well-developed case. Close agreement with linear theory (shown dotted) is apparent except at the highest frequencies. There are three possible reasons for the observed lower wavenumbers above frequencies of 1 Hz: (i) wind drift current, (ii) amplitude dispersion, and (iii) Doppler shifting of the highest wavenumbers above the Nyquist frequency, thereby lowering the average wavenumber. The effect of Doppler shifting may be clearly seen by separating the estimates of wavenumber into two classes depending on the instantaneous surface elevation, η: $\eta > (\overline{\eta^2})^{1/2}$ and $\eta < -(\overline{\eta^2})^{1/2}$. These classes correspond to the crests and troughs, respectively, of the largest waves. The resulting average wavenumbers in these classes are, respectively, lower and higher than the linear theory values, corresponding to forward advection on the crests and backward advection in the troughs as expected.

d. *Group structure*

Our hypothesis, that waves propagate in groups with significant energy concentrated in a narrow wavenumber band, may be tested by examining the time history of wavenumber magnitudes and directions. Figure 11 shows the evolution of amplitudes and wavenumbers during the passage of a group. The wave components at contiguous frequency bands, shown here by the different lines (0.50, 0.55, 0.60, 0.65 Hz), are the ones

that have consistent directions and whose amplitudes reflect the group shape. The propagation directions are shown in Fig. 11d and the amplitudes in Fig. 11b. The consistent tracking of the directions is striking and the standard deviation of the directions among these four frequencies is about the same as the standard error of the measurement of direction at each frequency as determined from the 35 independent estimates of direction given by (9).

The evolution of amplitudes through this group is consistent with a group that is coalescing (Pierson et al. 1992); that is, the higher frequencies are more prominent at the start of the group and there is a smooth evolution toward the end of the group, where the lower frequencies are dominant. This bunching of energy-containing wavenumbers happens repeatedly throughout the record. Similarly, there are times (Fig. 11b) when the energy in a particular frequency or band of frequencies falls to very low values.

Figure 12 shows an example of a wave group obtained on the EKOFISK oil platform in the North Sea. A group of three waves in excess of 6 m were observed and the corresponding time-dependent amplitudes of four frequencies in the vicinity of the peak show the evolution of energy toward low frequencies with time. The relatively high speed of the lower frequencies leads to coalescence of the group and the probability of even higher waves at some distance beyond the sensor. This raises the possibility of using information obtained at one point to deduce the statistics of extremes of waves for some considerable distance upstream and downstream. The additional information may greatly improve the confidence limits on extrema.

Finally, we address the question of whether these groups are isolated events or typical aspects of the ocean surface. In Fig. 13, we plot the spectrum of $|W_{qp}|$ at the peak frequency for run 87082 (dashed line). This

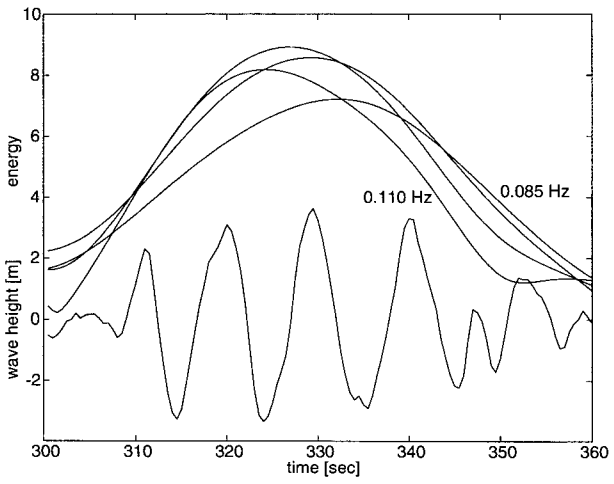

FIG. 12. The passage of a wave group as recorded on the EKOFISK oil platform in the North Sea, 93.01.12 at 1221 UTC.

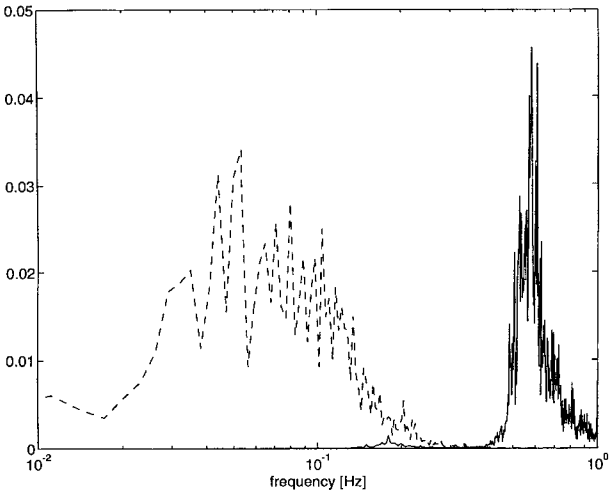

FIG. 13. Semilog plots of waveheight spectrum times frequency (solid line) and spectrum of $|W_{qp}|$ (times frequency) at the most energetic frequency for run 87082 (dashed line).

is an indication of the periodicity of groups around the peak frequency. Although broad compared to the wave spectrum (solid line in Fig. 13), there is a clear spectral peak around 0.05 Hz or 20 s, about 10 times the peak period, with significant energy between 40 s and 5 s. A more complete analysis of the group structure remains to be carried out, but this suggests that groups play an important role in the dynamics of the ocean.

5. Conclusions

We have proposed a way of viewing the underlying order in a chaotic wind-generated sea that has its antecedents in the group structure suggested by Mollo-Christensen and Ramamonjiarisoa. The analyzed data support this view and lead to a direct way of calculating directional properties of waves. The new results on directional spectra indicate that the most energetic waves are more focused than originally thought. Furthermore, the intermittent distribution of energy in any wavenumber band elucidates the process by which seas become steep and permits the calculation of extreme waves in a sea and other parameters of direct engineering interest. Perhaps most importantly, this new approach yields wavenumber spectra and wavenumber related time-dependent information, from which may be calculated surface properties of direct value to understanding the mechanics of remote sensing, gas transfer, and related fields.

Acknowledgments. We appreciate the support from the U.S. Office of Naval Research through Grant N00014-94-1-0629 to the National Water Research Institute. We gratefully acknowledge Bertrand Chapron, who provided the Morlet wavelet analysis routines, and Marshall Tulin and Gene Terray for many helpful dis-

cussions. We also thank Murray Poulter for providing the radar image shown in Fig. 1.

REFERENCES

Ataktürk, S. S., and K. B. Katsaros, 1987: Intrinsic frequency spectra of short gravity–capillary waves obtained from temporal measurements of wave height on a lake. *J. Geophys. Res.*, **92,** 5131–5141.

Capon, J., 1969: High-resolution frequency–wavenumber spectrum analysis. *Proc. IEEE,* **57,** 1408–1418.

Chapron, B., A. K. Liu, C. Y. Peng, and E. Mollo-Christensen, 1996: Higher order scale analysis. *The Air–Sea Interface,* M. A. Donelan, W. H. Hui, and W. J. Plant, Eds., University of Toronto Press, 335–340.

Donelan, M. A., and W. J. Pierson, 1987: Radar scattering and equilibrium ranges in wind-generated waves with application to scatterometry. *J. Geophys. Res.*, **92,** 4971–5029.

——, J. Hamilton, and W. H. Hui, 1985: Directional spectra of wind generated waves. *Philos. Trans. R. Soc. London,* **A315,** 509–562.

——, M. S. Longuet-Higgins, and J. S. Turner, 1972: Whitecaps. *Nature,* **239,** 449–451.

Farge, M., 1992: Wavelet transforms and their applications to turbulence. *Ann. Rev. Fluid Mech.*, **24,** 395–457.

Farmer, D. M., and S. Vagle, 1988: On the determination of breaking surface wave distributions using ambient sound. *J. Geophys. Res.*, **93,** 3591–3600.

Grossmann, A., and J. Morlet, 1984: Decomposition of Hardy functions into square integrable wavelets of constant shape. *SIAM J. Math. Anal.*, **15,** 723–736.

Hasselmann, K., 1962: On the non-linear energy transfer in a gravity wave spectrum. *J. Fluid Mech.*, **12,** 481–500.

——, 1974: On the spectral dissipation of ocean waves due to white-capping. *Bound.-Layer Meteor.*, **6,** 107–127.

——, and J. I. Collins, 1968: Spectral dissipation of finite-depth gravity waves due to turbulent bottom friction. *J. Mar. Res.*, **26,** 1–12.

Hayashi, T., 1994: An analysis of wind velocity fluctuations in the atmospheric surface layer using an orthogonal wavelet transformation. *Bound.-Layer Meteor.*, **70,** 307–326.

Hui, W. H., and J. Hamilton, 1979: Exact solutions of a three-dimensional nonlinear Schrödinger equation applied to gravity waves. *J. Fluid Mech.*, **93,** 117–133.

Kaiser, G., 1994: *A Friendly Guide to Wavelets.* Birkhäuser, 300 pp.

Komen, G. J., L. Cavaleri, M. Donelan, K. Hasselmann, S. Hasselmann, and P. A. E. M. Janssen, Eds., 1994: *Dynamics and Modelling of Ocean Waves,* Cambridge University Press, 560 pp.

Longuet-Higgins, M. S., 1952: On the statistical distributions of the heights of sea waves. *J. Mar. Res.*, **9,** 245–266.

——, 1983: On the joint distribution of wave periods and amplitudes in a random wave field. *Proc. R. Soc. London,* **A389,** 241–258.

——, and R. W. Stewart, 1964: Radiation stress in water waves; a physical description with applications. *Deep-Sea Res.*, **11,** 529–562.

Lygre, A., and H. E. Krogstad, 1986: Maximum entropy estimation of the directional distribution in ocean wave spectra. *J. Phys. Oceanogr.*, **16,** 2052–2060.

Magnusson, A. K., 1993: Modelling wave–current interactions. Ph.D. thesis. Geophysical Institute, University of Bergen, 79 pp.

Makin, V. K., 1979: The wind field above waves. *Oceanology,* **19,** 127–130.

Meyer, Y., 1989: Orthonormal wavelets. *Wavelets: Time-frequency Methods and Phase Space,* J. M. Combes, A. Grossmann, and P. Tchamitchian, Eds., Springer, 21–36.

Miles, J. W., 1957: On the generation of surface waves by shear flows. *J. Fluid Mech.*, **3,** 185–204.

Mollo-Christensen, E., and A. Ramamonjiarisoa, 1978: Modeling the presence of wave groups in a random wave field. *J. Geophys. Res.*, **83,** 4117–4122.

Neumann, G., and W. J. Pierson, Jr., 1966: *Principles of Physical Oceanography.* Prentice-Hall, 545 pp.

Phillips, O. M., 1957: On the generation of waves by turbulent wind. *J. Fluid Mech.*, **2,** 417–445.

——, 1958: The equilibrium range in the spectrum of wind-generated waves. *J. Fluid Mech.*, **4,** 426–434.

——, 1960: On the dynamics of unsteady gravity of finite amplitude. Part 1. *J. Fluid Mech.*, **9,** 193–217.

——, 1985: Spectral and statistical properties of the equilibrium range in wind-generated gravity waves. *J. Fluid Mech.*, **156,** 505–531.

Pierson, Jr., W. J., and W. Marks, 1952: The power spectrum analysis of ocean-wave records. *Trans. Amer. Geophys. Union,* **33,** 834–844.

——, M. A. Donelan, and W. H. Hui, 1992: Linear and nonlinear propagation of water wave groups. *J. Geophys. Res.*, **97,** 5607–5621.

Poulter, E. M., M. J. Smith, and J. A. McGregor, 1995: S-band FMCW radar measurements of ocean surface dynamics. *J. Atmos. Oceanic Technol.*, **12,** 1271–1286.

Ramamonjiarisoa, A., 1974: Contribution à l'étude de la structure statistique et des méchanismes de génération des vagues de vent. Ph.D. thesis, Université de Provence (IMST no. A.O. 10023), 181 pp.

Toba, Y., 1973: Local balance in the air–sea boundary processes. Part III: On the spectrum of wind waves. *J. Oceanogr. Soc. Japan,* **29,** 209–220.

Tolman, H. L., 1991: A third-generation model for wind waves on slowly varying, unsteady, and inhomogeneous depths and currents. *J. Phys. Oceanogr.*, **21,** 782–797.

Tsanis, I. K., and F. P. Brissette, 1992: Wave directional spectra measurements by small arrays in Lake Ontario. *J. Great Lakes Res.*, **18,** 489–506.

Yuen, H. C., and B. M. Lake, 1975: Nonlinear deep water waves: Theory and experiment. *Phys. Fluids,* **18,** 956–960.